Better Operational Forecasting for the Contemporary Arctic via Ocean Wave Integration

Vernon A. Squire
Department of Mathematics and Statistics, University of Otago, Dunedin, New Zealand
Timothy D. Williams
Nansen Environmental and Remote Sensing Center, Bergen, Norway
Luke G. Bennetts
School of Mathematical Sciences, University of Adelaide, Australia

ABSTRACT

Whether configured for operational purposes or for research, current coupled ice-ocean models and oceanic global circulation models lack sophistication in regard to core aspects of sea ice behavior, notably the determinative contribution that ocean waves make in evolving the sea ice canopy and hastening its annihilation. Considerably enhanced climate resolving accuracy and reliability can potentially be achieved by incorporating naturally pervasive ocean wave / sea ice interactivity into a state-of-the-art polar ocean modeling framework originally developed and hosted by NERSC in Norway. This paper focuses on how to do this, recognizing the benefits that will flow from the research through better model parameterization and forecasting precision – especially with reference to contemporary adverse global warming effects.

KEY WORDS: Sea ice, global warming, operational ice-ocean forecasting, ocean wave scattering, Arctic and Subarctic seas, Southern Ocean, sea ice morphology adjustment.

INTRODUCTION

Recently, a sequence of publications has appeared that focuses on how natural ocean waves interact with polar sea ice in its several forms: quasi-continuous sheets, broken-up pack ice characteristic of the MIZ[1] and pancake ice slurries (Liu and Mollo-Christensen, 1988; Melsom, 1992; Shen and Squire, 1998; Squire, 2007; Squire et al., 1995; Weber, 1987). Considerable work has been done to understand scattering from various sea ice irregularities, e.g. cracks, open or refrozen leads, floe edges, changes in material property or thickness, pressure ridges, etc. (Bennetts and Squire, 2012b; Vaughan and Squire, 2007; Vaughan et al., 2007; Williams and Squire, 2004, 2006, 2007) and on ocean wave propagation through open ice fields such as MIZs (Bennetts et al., 2010; Bennetts and Squire, 2009, 2010; Bennetts and Williams, 2010). In addition, these elemental studies have been brought together to replicate how waves travel through large swathes of quasi-continuous natural sea ice that include an authentic distribution of leads and a representative empirical topography (Mahoney et al., 2007) found by submarine upward-looking sonar (Squire et al., 2009; Vaughan et al., 2009). Comparable progress has been made in the MIZ too (Bennetts et al., 2010; Bennetts and Squire, 2012b; Kohout and Meylan, 2008), where the FSD[2] is caused primarily by ocean waves. As waves penetrate the ice pack they are scattered by the floes, losing energy with distance traveled. On entry, they are powerful enough to fracture and at times pulverize local ice into slurry, a little further in they usually break up floes, but deeper in still the waves have become sufficiently emaciated that they no longer regulate floe size (Squire and Moore, 1980; Toyota et al., 2011, 2006; Wadhams et al., 1987). Beyond the fractured zone (Vaughan and Squire, 2011) the ice is quasi-continuous – ice floes are customarily larger though still punctuated by cracks, pressure ridges and leads. Scattering continues to take place at these heterogeneities but, because they are less abundant, other mechanisms such as sea ice inelasticity, turbulence, viscous damping in the water and collisions between floes can dominate. An alternation prevails, where the sea ice influences the incoming ocean waves and swells and the waves reshape the undergirding structure of the MIZ by regulating floe diameter through fracture.

Despite the patently intimate relationship between ocean waves and sea ice, their effect is not yet built into operational ice-ocean forecasting models and OGCMs[3]. This is of major importance to every maritime endeavor in each polar or subpolar sea, notably in regard to the safety of ships engaged in fisheries, tourism and geophysical or hydrographical prospecting, and Arctic offshore enterprises allied to hydrocarbon exploration. Vital operational

[1] Marginal ice zone, the 10s–100s km wide outer part of the pack ice cover that interacts with the open ocean, comprising a mélange of dispersed floes and cakes a few meters across near the ice edge but increasing in size with penetration

[2] Floe size distribution

[3] Oceanic global circulation models

forecasts to support these activities are currently deficient, as they neglect a fundamental physical process that profoundly affects the sea ice cover. Moreover, the well-documented reductions in ice thickness, extent and concentration in the summer Arctic Ocean (Holland et al., 2006; Kwok and Rothrock, 2009; Serreze et al., 2007; Wadhams and Davis, 2000), which have caused the ice to become more like a MIZ, and the redistribution of sea ice morphology in the Southern Ocean, indicate that ocean waves will now exert a much greater influence than hitherto. This change will be fueled by the heightened and more extreme meteorological events that we continue to experience due to climate change, leading to higher waves being created at distant storm centers that then advance into the ice cover. But it will also be affected by the greater fraction of open sea within ice fields, which will promote the generation of waves in situ by increasing fetch. The intensification will act in two ways: it will fashion a distribution of floe sizes that is biased towards much smaller ice floes by fracturing any floe that flexes beyond its failure strength, as described above; and, by introducing local warm surface water to the now broken up mass of smaller ice floes and cakes (Gladstone et al., 2001; Wadhams et al., 1979), the waves will promote melting on top of the thermal assault due to enhanced shortwave absorption arising from ice-albedo feedback. As a consequence, ocean waves will nourish the positive feedback that occurs because of albedo adjustment.

The overarching end goal of this paper is thus to enhance the accuracy and performance of large-scale coupled ice-ocean models and, prospectively, OGCMs, by taking into account the ubiquitous appreciable influence of ocean waves on sea ice fields for the first time. Our project will potentially deliver a global observational and modeling capability with markedly improved performance and accuracy because (i) no observation system exists of waves in ice fields, either for quasi-continuous sea ice or MIZs; (ii) operational wave models don't simulate wave propagation into ice infested areas; and (iii) ice-ocean models don't include waves despite their influence on sea ice dynamics. Furthermore, it will also allow calculations and forecasting of ocean waves propagating in the polar oceans to be made, including how the sea ice is modified by their presence, e.g. broken up and, by this means, encouraged to melt more rapidly.

The paper begins by focusing on two (linked) aspects of ocean wave / sea ice interactivity, namely the attenuation experienced by waves due to systematic scattering by ice floes including its sensitivity to ice morphology (Bennetts and Squire, 2012a,b), and the breakup of those floes when they are strained beyond their point of failure (Langhorne et al., 1998, 2001; Vaughan and Squire, 2011; Williams et al., 2012). Results are then presented that accommodate one-dimensional ocean wave / sea ice interaction (Dumont et al., 2011; Williams et al., 2013a,b) and some preliminary results with two-dimensional interactions (Williams et al., 2012); both for the Fram Strait region in the north Greenland Sea.

WAVE ATTENUATION

Ocean surface waves attenuate in ice-covered seas because of the nature of the sea ice encountered during their passage, including scattering from the edges of floes and irregularities such as pressure ridges and cracks, and because of supplementary energy dissipation mechanisms such as irreversible ice deformation, turbulence in the water and ice floe collisions when the seas are rough. The reduction in amplitude is observed to be exponential, with an attenuation coefficient that decreases as wave period τ increases (Squire and Moore, 1980; Wadhams et al., 1987). Bennetts and Squire (2012b) model the observed exponential attenuation, seeking parsimonious averaging methods for obtaining the attenuation coefficient for each type of feature sought, including aggregations of those features, plus a parameterization of the supplementary damping. Like the current paper, Bennetts and Squire's investigation is motivated by a drive for efficiency, as the principal incentive for their work is to embed wave interactions in a computationally intensive ice-ocean model. For this reason an appealing alternative option is to parameterize ocean wave / sea ice interactions across the entire ice field, e.g. using a spatially-variable nonlinear viscoelastic rheology that accurately reproduces dispersion, attenuation and breakup. But, despite some preliminary progress with this approach (Wang and Shen, 2010, 2011), the calibration of the viscoelastic moduli represents a massive challenge that is in all probability impracticable. Notwithstanding this, the major objective remains to accurately represent the interactions of waves with local sea ice fields as they travel from grid cell to grid cell in an ice-ocean model.

Preliminaries

On account of the strain rates involved, the presence of ice on the surface of the ocean is customarily modeled as a thin elastic plate when it is interacting with surface gravity waves. Combining this with the linearized Bernoulli pressure equation and assuming no cavitation where the ice and water meet, provides the coupling between the surface displacement w and a velocity potential $\phi(x,z)$ that satisfies Laplace's equation for the underlying water of depth H. A second kinematic coupling equation, a seafloor impermeability condition, and radiation conditions in the far field close the system. When ice is not present, $\phi(x,z)$, truncated at some integer value N chosen to be sufficiently large to obtain a desired accuracy, takes the form

$$\phi(x,z) \approx \sum_{n=0}^{N} (a_n \mathrm{e}^{\mathrm{i}k_n x} + b_n \mathrm{e}^{-\mathrm{i}k_n x}) \cosh k_n(z+H), \tag{1}$$

where x and z are the horizontal and vertical (upward from free surface) coordinates respectively, and a_n and b_n are amplitudes that depend on the surrounding geometry. The quantities k_n are wave numbers that are calculated as the roots k of the free-surface dispersion relation $k \tanh kH = \omega^2/g$, with k_0 denoting the primary traveling wave mode in water and the angular frequency $\omega = 2\pi/\tau$. The subsequent wave numbers, k_n $(n = 1, 2, \ldots)$, lie on the positive imaginary axis and are ordered in increasing magnitude. They support evanescent waves that are generated by sea ice features and decay exponentially in the water with distance away from them. In intervals of constant ice thickness D, the velocity potential has the form

$$\phi(x,z) \approx \sum_{n=-2}^{N} (\alpha_n \mathrm{e}^{\mathrm{i}\kappa_n x} + \beta_n \mathrm{e}^{-\mathrm{i}\kappa_n x}) \cosh \kappa_n(z+H), \tag{2}$$

with amplitudes α_n, β_n. The wave numbers κ_n are then the roots κ of the dispersion relation

$$(1 - \omega^2 d/g + F\kappa^4)\kappa \tanh \kappa(H-d) = \omega^2/g \tag{3}$$

for an ice cover of draft d and scaled effective (low strain rate) flexural rigidity F (see Bennetts and Squire, 2012b), with κ_0 denoting the primary traveling wave mode in the ice. The wave numbers κ_n $(n = 1, 2, \ldots)$ lie on the positive imaginary axis. However, the high-order boundary condition produced by the presence of ice,

generates two additional wave numbers, κ_{-n} $(n = 1, 2)$. These wave numbers exist in the upper-half complex plane and are typically mirror images of one another in the imaginary axis. In this case they support damped propagating waves.

No wave energy is lost when the overall system as described above is used; however, recall that inelasticity and turbulence produce dissipation. This can be parameterized by including an extra imaginary term in the dispersion relation that arises from an extra velocity-dependent term in the plate equation (Robinson and Palmer, 1990).

Bennetts and Squire (2012b) define a floe as a finite stretch of uniform sea ice that is disconnected from other ice by open water; a crack as the outcome of the open water between two ice sheets closing to zero; and a pressure ridge as a finite interval of variable thickness separating two ice sheets. Their aim is to determine the attenuation produced by a large but finite number M of each of these individual features.

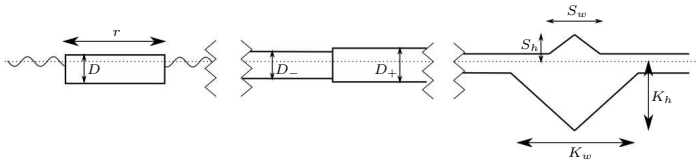

Fig. 1. Some ice features considered by Bennetts and Squire (2012b), with notation. From left to right: a floe, a crack and a first-year pressure ridge with profile consistent with Timco and Burden (1997).

Single Features

This paper focuses on scattering within two types of sea ice cover particularly; MIZs composed of many individual floes, and more continuous ice populated by cracks and pressure ridges. Including parameterized damping, Bennetts and Squire (2012b) deal with each scatterer, i.e. floes, cracks and ridges (Fig. 1), in considerable detail so it is unnecessary to do this here. But briefly,

(a) The attenuation coefficient can be found from the canonical problem of wave scattering at a single ice edge when floes are of sufficient length that a wide spacing approximation (WSA)[4] is valid.
(b) On the whole, transmission through a crack gradually increases with wave period but, because of the perfect geometry, a unique resonant period at a position that depends on ice thickness also exists where transmission is perfect. Ensemble averaging over many crack simulations suppresses this undesirable artifact. Because cracks have no length, viscous damping has minimal effect and can be ignored.
(c) No averaging of the properties of pressure ridges appears to be required for either first-year ridges (shown in Fig. 1) or multi-year ones, and damping needs to be considered only rarely.

Further investigations of single features, this time centered on sensitivity to physical parameters, have also been done by Bennetts and Squire (2012a). In the context of scattering by floes, for example, they have looked at how the energy reflected by a single ice floe is affected by the effective Young's modulus (Fig. 2) and found that reflection increases by approximately an order of magnitude as the modulus increases over its range and that the maximum occurs at a wave period that increases with ice thickness D. Bennetts and Squire (2012a) also investigate, as a function of wave period, the sensitivity of the attenuation coefficient to the geometrical descriptors of various scatterers, e.g. ice thickness or ridge width, and they consider the effect of roughness.

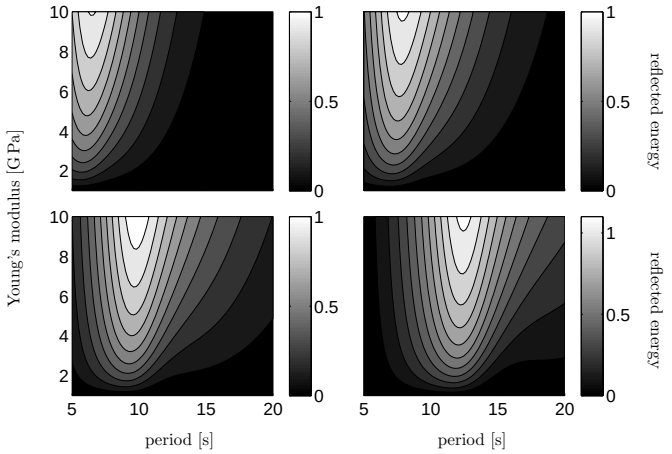

Fig. 2. The energy reflected by a single ice edge against wave period and the effective modulus. The contour values at each period are scaled by the values for the smallest modulus in the range considered, i.e. 1 GPa, and are on a $\log_{10}$ scale. $D = 0.5$ m (top-left panel), 1 m (top-right), 2 m (bottom-left) and 4 m (bottom-right).

Multiple Features

Wave scattering involves an infinite sequence of reflections between any two interfaces and, as explained by Berry and Klein (1997), exponential decay follows as a result of wave coherence, i.e. phase interactions, and positional disorder, i.e. it is a localization effect. For multiple features the property is visible in the results of Kohout and Meylan (2008) and Bennetts and Squire (2012b), for both open ice fields and quasi-continuous ice. It is computationally expensive to replicate because the scattering properties of a large number of individual features must be found, combined for the set of features, and then repeated a large number of times to form an ensemble.

MIZs. Bennetts and Squire (2012b) show that a WSA gives excellent agreement with the complete solution which fully incorporates evanescent oscillations in the water that interact with the next scattering interface encountered.

The WSA enables the use of an averaging technique proposed by Berry and Klein (1997), conceived to describe the scattering of optical waves. It allows the ensemble average of the attenuation produced by any number of scatterers, i.e. the geometrically (logarithmically) averaged transmission, over all possible phases, to be found from the properties of the individual scatterers. Applied to a transect of M floes, the resulting expression is

$$\exp\{\langle\langle \log |T_{1,M}|^2\rangle\rangle\} = \exp\{M\langle \log |T_0|^2\rangle\}. \tag{4}$$

On the left-hand side of the above identity $|T_{1,M}|^2$ is the energy transmitted by the floes and $\langle\langle\cdot\rangle\rangle$ denotes the ensemble average over phases and the properties of the floes, i.e. thickness and length. On the right-hand side $|T_0|^2$ is the energy transmitted by a single floe and $\langle\cdot\rangle$ denotes the ensemble average over its

[4] Wave modes other than those corresponding to the primary propagating mode are neglected

properties. The corresponding attenuation coefficient is therefore given by the simple expression

$$\mu = -\langle \log |T_0|^2 \rangle, \tag{5}$$

where μ is with respect to the number of scatterers and hence is nondimensional. Averaging over the thickness of the floe makes little difference to the results, and $\langle \cdot \rangle$ thus becomes an average over floe length only. Applying a WSA to the floes themselves and again using the technique of Berry and Klein (1997), the above expression for the attenuation coefficient can be reduced further to

$$\mu = -2 \log(1 - |R|^2), \tag{6}$$

where $|R|^2$ is the wave energy reflected by an ice edge of the average thickness. The dimensional attenuation coefficient u, defined with respect to distance into the ice cover, is given by $u = \mu c/l$, where c is the ice concentration and l is the average floe length. A similar expression to Eq. 6 was used by Williams and Squire (2010) for estimation of the thickness of an ice sheet containing multiple cracks.

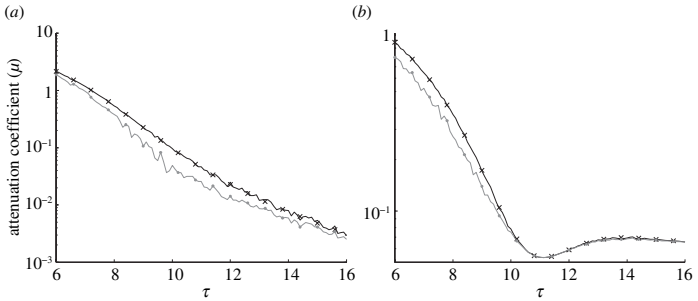

Fig. 3. The attenuation coefficient as a function of wave period τ. (a) A MIZ with identical floes of length 100 m and $D = 3$ m. (b) Quasi-continuous ice of 3 m thickness containing cracks, where the primary wave number is given an imaginary component of magnitude 10^{-4} to include viscosity. In both cases the WSA is used to calculate the wave interactions between features and the distribution of their separations is uniform over half a wavelength. The solid curves show results calculated using ensembles with arithmetic (light grey, dotted) and geometric (i.e. logarithmic, black) averaging. The crosses are semi-analytic expressions.

Fig. 3a compares the attenuation coefficients produced by standard averaging, as used by Kohout and Meylan (2008), and geometric averaging. Although there is a clear gap between the values given by the two averaging methods, particularly for the mid-range periods, the attenuation coefficients are similar both qualitatively and quantitatively, and to the first significant figure. Expression 6 is overlaid on the figure as crosses and is close to the values calculated by ensemble averaging, with noise from the latter being the only visible difference.

Quasi-continuous sea ice. Wave interactions between imperfections in near continuous ice sheets, e.g. cracks and pressure ridges, must be considered separately to those that occur between floes in the MIZ because of the presence of damped-propagating waves in intervals of ice-covered fluid (the 'extra' $n = -2, -1$ modes in Eqs. 1 and 2). Unfortunately, numerical investigations suggest that the damped-propagating waves can have a significant effect on interactions between features. For repeated cracks at modest separations there are clear qualitative and quantitative differences between WSA results and those that include the $n = -2, -1$ modes, which are greatest when the wave period τ is small and the sea ice is thick. Naturally, as separation increases the WSA does a better job. It appears that damped-propagating waves are the dominant additional contributors to wave interactions at small separations but, in contrast to the MIZ, it is also necessary to include a number of the evanescent modes, i.e. $n = 1, 2, \ldots$ in Eq. 2 to eliminate spurious resonant effects that lead to inaccuracies in the transmitted energy. For realistic pressure ridges, the effect of not including the $n = -2, -1$ modes is less pronounced than that for cracks; indeed there is no visible difference between the WSA and the approximation that includes the damped-propagating waves even when the ridges are quite close.

In reality, most pressure ridges are separated (peak to peak) by 80 to 300 m (Davis and Wadhams, 1995), while, based on leads which are more easily detected, the separation of cracks is typically of the order of kilometers (Sear and Wadhams, 1992). In practice, it is reasonable, therefore, to use a WSA to calculate wave interactions between cracks and ridges as well as floes, except where features are closely spaced when additional modes $n = -2, -1, 1, 2, \ldots$ in Eq. 2 are necessary for accuracy.

Accordingly, the WSA results of Fig. 3b are for 3-m-thick quasi-continuous ice containing uniformly distributed cracks, with some parameterized damping of the primary wave number. Crack separation is evidently a determinant of the attenuation rate. Results are again shown for the arithmetic and geometric means, using ensemble averages. The semi-analytic expression 6 is also overlaid. It is clear that damping dominates at larger wave periods, where the arithmetic and geometric averages coincide, while scattering at cracks is more important at lower periods. The clear minimum at approximately 11 s corresponds to perfect transmission by individual cracks, a sensitivity to the geometrical configuration that is reduced by averaging.

Eddy viscosity Following Robinson and Palmer (1990), Bennetts and Squire (2012b) introduced an eddy viscosity parameter Γ into (3) to produce additional attenuation that brings the damping of long waves more into line with field observations (Squire and Moore, 1980), i.e.

$$(1 - \omega^2 d/g + F\kappa^4 - \mathrm{i}\omega\Gamma)\kappa \tanh \kappa(H - d) = \omega^2/g. \tag{7}$$

If $\tilde{\kappa}_0$ is the closest root to κ_0, then the dimensional attenuation coefficient becomes $u = c(\mu/l + 2\delta)$, where $\delta = \Im\mathfrak{m}[\tilde{\kappa}_0] > 0$.

FSD AND BREAKUP

Observations

Observations of floe sizes in Arctic areas suggest that they generally follow a power law (Pareto) distribution with an infinite maximum floe size. However, many of the observations are theoretically problematic, as the empirically fitted exponent γ in the distribution is often found to exceed 2 which implies an infinite ice area if small floes obey this law. Toyota et al. (2006) investigated the FSD for small floes in the Sea of Okhotsk, and found γ decreased to about 1.15 when floe diameter was less than about 40 m, the size below which flexural failure does not occur. The same effect was seen in the Weddell Sea and off Wilkes land during late winter (Toyota et al., 2011). Toyota et al. conclude that the smaller floes are mainly produced by ocean wave induced fracture, while larger ones are more influenced by large scale stresses in the ice cover that arise from winds and currents.

Ice rubble near the edge probably arises from collisions between floes induced primarily by waves also.

Breakup

Failure strain and flexural strength. Unfortunately, the failure strain of sea ice ϵ_c has not been measured often. Indeed to the authors' knowledge, there are only two field experiments where this has been done, which both suggest an ϵ_c value in the vicinity of $(5 \pm 3) \times 10^{-5}$. In contrast, many flexural strength tests have been made due to its importance and use in ice engineering. Yet sea ice is a heterogeneous aggregate of solid ice, brine, air and solid salts, so flexural strength is not a basic material property and it is not equal to tensile strength as it would be for homogeneous materials. It is an indicial strength, as non-uniform stress fields are created under flexural loads that require assumptions about material behavior. Timco and O'Brien (1994) collate and analyse nearly a thousand flexural strength measurements to show that the flexural strength σ_c has a very simple dependence on brine volume fraction υ_b, namely $\sigma_c = 1.76 \exp(-5.88\sqrt{\upsilon_b})$ MPa, which decreases monotonically as υ_b increases. Brine volume is usually found from a standard formula by measuring salinity and temperature in situ using coring and thermistor or thermocouple probes.

To convert σ_c to ϵ_c is, in principle, straightforward as for an elastic beam

$$\epsilon_c = \frac{\sigma_c}{Y}, \tag{8}$$

where Y is the (dynamic) Young's modulus. However, the constitutive relation for sea ice is rate dependent and, as well as the elastic strain, it includes primary, secondary and tertiary creep. For the strain rates associated with ocean wave / sea ice interactions only the first and second of these deformations are important, which are often called the instantaneous elastic and delayed elastic (anelastic) strains, denoted ϵ^i and ϵ^d, so the total recoverable strain is $\epsilon^i + \epsilon^d$. Accordingly, the same Eq. 8 can be used to find ϵ_c from σ_c but with a reduced value for Young's modulus; the so-called effective modulus referred to earlier. A reduction of 1 GPa is justified by Williams et al. (2013a,b) to take account of ϵ^d, along with a reduction of $\sim$ 2–4 GPa because of the presence of brine in the sea ice (Timco and Weeks, 2010), noting that data describing how the effective modulus depends on brine content are quite scattered. Fortunately, the failure strain found from the many flexural strength observations in the sea ice literature (Timco and O'Brien, 1994) are in concert with the few data that are available on fracture strain.

Finding the ice strain due to waves. Equipped with a strain value for when sea ice will break we can now determine whether ice floes will survive the onslaught of water waves of amplitude $A(\omega)$ at any point within the MIZ or in the ice interior, by comparing the maximum wave-induced flexural ice strain to that required for the ice to fail. A relatively simple way to proceed assumes a sinusoidal wave profile $w = A(\omega)W(\omega)\cos(\kappa_0 x - \omega t)$ traveling through the ice on infinitely deep water, where $W(\omega) = (g\kappa_0/\omega^2)|T|$, κ_0 is found from the ice-covered dispersion relation (3), and $|T|$ is the transmission coefficient for a wave traveling from open water into ice (see, e.g. Williams and Porter, 2009). The maximum strain in the ice can be approximated by

$$\epsilon_{max} = A\epsilon_A, \tag{9}$$

where $\epsilon_A(\omega) = DW\kappa_0^2/2$ is the strain per meter of wave amplitude. The spectral density function for the strain in the ice will then be $S(\omega)\epsilon_A^2$, where S here designates a general wave spectrum that produces the local open water displacement. This may be in the open ocean or within the MIZ after attenuation has occurred.

An alternative approach, due to Dumont et al. (2011), is to use flexural strength directly and to assume that the ice doesn't necessarily conform to the shape of the wave. However, this assumption leads to a counterintuitive outcome for very long waves of low curvature where the ice must deform to the wave to satisfy Hooke's law, namely that very long waves require only a very small amplitude to break the ice.

Probability. The wave amplitude A is generally assumed to follow a Rayleigh distribution, so it is reasonable to assume that the strain amplitude, denoted E, follows one too. That is, for prescribed A_c and ϵ_c,

$$\mathbb{P}(A > A_c) = e^{-A_c^2/2\langle w^2\rangle}, \quad \mathbb{P}(E > \epsilon_c) \equiv \mathbb{P}_\epsilon = e^{-\epsilon_c^2/2\langle\epsilon^2\rangle}, \tag{10}$$

where

$$\langle w^2\rangle = \int_0^\infty S(\omega)\mathrm{d}\omega, \quad \langle\epsilon^2\rangle = \int_0^\infty S(\omega)\epsilon_A^2\mathrm{d}\omega \tag{11}$$

are respectively the mean square wave displacement of the ice and the mean square wave strain. The commonly defined significant wave height $H_s = 4\sqrt{\langle w^2\rangle}$ and the significant strain amplitude $E_s = 2\sqrt{\langle\epsilon^2\rangle}$. Therefore, the criterion $\mathbb{P}_\epsilon > \mathbb{P}_c$ can be written in terms of E_s, ϵ_c and $\mathbb{P}_c$ as

$$E_s > E_c = \epsilon_c\sqrt{-2/\log(\mathbb{P}_c)}. \tag{12}$$

Thus the single parameter E_c combines the effects of both ϵ_c and $\mathbb{P}_c$. If $\mathbb{P}_c = e^{-2} \approx 0.14$, then we get the criterion of Langhorne et al. (2001), i.e. $E_s > \epsilon_c$, which also corresponds to the upper limit tested by Vaughan et al. (2009). Notwithstanding, the default value for $\mathbb{P}_c$ that is used in our numerical results is based on the condition for a narrow spectrum. For a monochromatic wave that produces a strain amplitude E_w, the breaking condition would be $E_w > \epsilon_c$. Therefore, since $\langle\epsilon^2\rangle = E_w^2/2$ in that case, the breaking condition is $E_s > \epsilon_c\sqrt{2}$. This corresponds to choosing $\mathbb{P}_c = e^{-1} \approx 0.37$ in (12). We note that this value is easily changed in our model when more theoretical and observational information become available.

ICE-OCEAN MODEL

Processing Steps

Given a prescribed directional spectral density function in open water $\mathcal{S}(\omega,\theta)$ we are now in a position to propagate it into the ice. We do this according to the equation (see, e.g. Perrie and Hu, 1996)

$$\frac{1}{c_g}D_t\mathcal{S}(\omega,\theta) \equiv \frac{1}{c_g}\left(\partial_t + \mathbf{c}_g\cdot\nabla\right)\mathcal{S}(\omega,\theta) = -u(\omega)\mathcal{S}(\omega,\theta), \tag{13}$$

where the group velocity $c_g = \mathrm{d}\omega/\mathrm{d}\kappa_0$ and $\mathbf{c}_g = -c_g(\sin\hat{\theta}, \cos\hat{\theta})^T$, where $\hat{\theta} = \pi\theta/180^\circ$ is the direction the wave is coming from, measured clockwise from north. The right-hand-side of our equation (13) is simpler than that of Perrie and Hu (1996), who allowed for angular diffraction of waves inside the ice and also for other effects like wave generation by wind and wave breaking. One consequence of this is that waves do not change direction once they leave the wave mask.

To solve (13) numerically we take the approach of Dumont et al. (2011) and map $\mathcal{S}(\omega,\theta)$ onto an intermediary advected spectrum

$\tilde{\mathcal{S}}(\omega,\theta)$ at each grid cell (by solving $D_t\tilde{\mathcal{S}}=0$), and then attenuate the spectrum using $\mathcal{S}(\omega,\theta)=\tilde{\mathcal{S}}(\omega,\theta)\exp(-uc_g\Delta t)$. (The initial value of $\mathcal{S}(\omega,\theta)$ is usually provided parametrically by a wave model such as WAM.) The steps above give the new value of $\mathcal{S}(\omega,\theta)$, which is used to determine if breaking occurs and is then carried forward to the next time step. The attenuation coefficient u is taken from a pre-calculated look-up table drawn from the model of Bennetts and Squire (2012b), and depends upon the ice concentration and thickness.

To determine if breaking occurs we first calculate the frequency spectrum $S(\omega)=\int_0^{2\pi}\mathcal{S}(\omega,\theta)\mathrm{d}\hat{\theta}$, which allows us to compute E_s. The average time between waves (Williams et al., 2013a) for our time interval is

$$\tau_w=2\pi\sqrt{\frac{m_0}{m_2}},\quad m_n=\int_0^\infty\omega^nS(\omega)W(\omega)\mathrm{d}\omega,$$

which lets us estimate a typical wavelength λ_w. If E_s is big enough, we reduce the maximum possible floe size ($l_{\max}$) in each grid cell to half that wavelength, so long as it is greater than 20 m, compute a new mean floe size l for the cell, and step forward in time. (To determine l from $l_{\max}$, we take the approach of Dumont et al. (2011) and assume the FSD is produced by fractal breaking.) By this means the FSD gradually evolves in response to the incoming ocean wave field $S(\omega)$, as is observed, and MIZ width is determined by the destructive ability of $S(\omega)$ to break up floes up to a certain distance into the ice field.

Preliminary results

These results update those of Williams et al. (2012). Both assume the incident wave spectrum S is a Bretschneider spectrum, with directionality added (where present) using a $\cos^2$ spreading function. Fig. 4 uses Fig. 7(a,d) of Williams et al. (2013b). For a one-dimensional S, it shows the sensitivity of the width of the MIZ to the breaking strain and the eddy viscosity parameter. As expected, decreasing ϵ_c increases MIZ width. There is significant variation among the results which suggests that good estimates for the ice properties are important. It also shows that increasing the thickness from 2 m to 3 m reduces the MIZ width by about $\frac{2}{3}$ due to increased attenuation (compare the red curve in (a) with the blue curve in (b)). Hence reliable thickness data (whether modeled or measured) are also very important.

Similarly, decreasing the attenuation by reducing Γ also increases the MIZ width. There is again considerable variation in the results making the improved modeling of the attenuation of long waves a high priority for future work.

Fig. 5 shows some preliminary two-dimensional results. A high-resolution model of the Fram Strait is run using boundary conditions from the 15 km-resolution TOPAZ model (Sakov et al., 2012). In all figures, dark-grey areas represent land. All the waves travel at the same speed $c_g=0.7\times\min\{\Delta x\}/\Delta t$, where $\min\{\Delta x\}\approx3.4$ km here, and $\Delta t=128.7$ s. As shown by Williams et al. (2013b), a Courant number of 0.7 should be small enough to let the wave spectrum form an equilibrium with this degree of floe breaking. The aforementioned paper also shows that neglecting dispersion should have little impact on the calculated MIZ width of 24 km (calculated by adapting the method of Strong, 2012).

In (b) and (c), we do not plot H_s itself, but instead an effective significant wave height, H_s'. Inside the wave mask, this is less than H_s since we do not integrate $\mathcal{S}$ over the full range of directions. Thus, $(H_s'/H_s)^2$ can be thought of as representing the fraction of

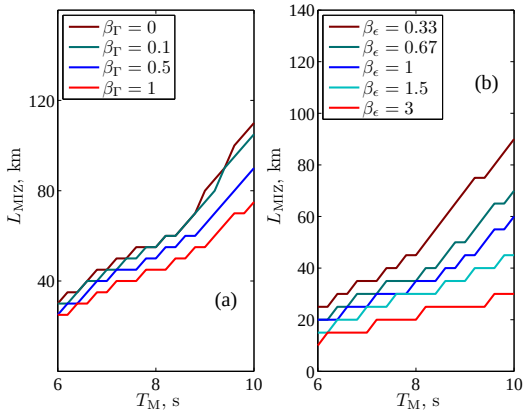

Fig. 4. Variation of MIZ width L_{MIZ} with peak spectral period T_{M} for different values of the eddy viscosity parameter Γ and failure strains ϵ_c. In (a) $D=2$ m, $\epsilon_c=4.99\times10^{-5}$, and $\Gamma=(10\beta_\Gamma)\,\mathrm{Pa\,s\,m^{-1}}$. In (b) $D=3$ m, $\Gamma=10\,\mathrm{Pa\,s\,m^{-1}}$, and $\epsilon_c=4.99\times10^{-5}\beta_\epsilon$. In all plots the concentration is uniformly 0.8 and the incident significant wave height is 3 m.

energy traveling into the ice. In this simulation, we also constrain $\mathcal{S}$ to agree with the WAM model at $t=0$ and $t=24$ h, and interpolate linearly between these times. This stops too much error creeping into the waves in the wave mask due to the physics neglected in (13).

Using moored upward looking sonar data, Vinje et al. (1998) constructed time series of ice thickness in Fram Strait by measuring ice draft every 4 minutes, i.e. a nominal sampling interval of 30 m. These authors found that the modal ice thickness has a maximum of 3.15 m in May and a minimum in September of 2.43 m, an annual variation range of 0.72 m. This compares well with early model results, comprehensive drillings, and most of the submarine observations during the 2–3 decades prior to the Vinje et al. dataset, indicating no significant long-term ice thickness change up to 1998. (This date is close to our HYCOM simulations of 3 January 2000, so our average thickness, after being doubled, of 2.0 m is not unreasonable.) The calculated median MIZ width of 24 km from (d) is probably too small for this time of year but in this case it could be partly attributed to the restricted model domain, as the waves are mainly coming from the south leading to much of the ice being shielded from the waves. This situation could be improved by fully implementing the transfer of $l_{\max}$ and $\mathcal{S}$ from the outer TOPAZ model to the Fram Strait model. Also, as shown by Fig. 4, uncertain ice properties like D, ϵ_c and Γ can make a significant difference, as can daily variations in the incident wave field.

CONCLUSIONS

While the results presented in this paper are preliminary, the authors wish to stress again the substantial effect that waves have on the morphology of the marginal ice zone and, consequently, on air/sea interaction. In a nutshell, ocean waves penetrating ice fields regulate the floe size distribution by fracturing ice floes that are too large to exist at their specific locations, noting that the ice itself scatters and attenuates the waves as they pass by. Along with currents and winds, waves also cause the ice to move laterally and they promote melting. Because global climate change has raised the frequency of extreme events and increased the fetch lengths within ice fields by lowering concentration, the capacity

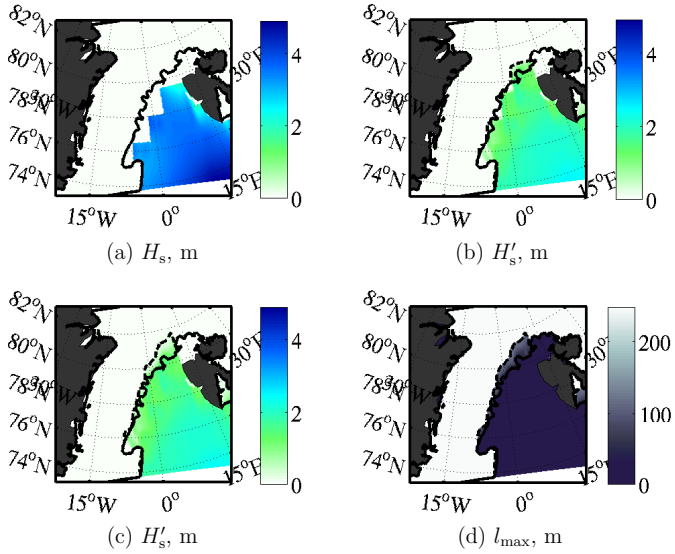

(a) H_s, m (b) H'_s, m

(c) H'_s, m (d) l_{max}, m

Fig. 5. Preliminary two dimensional results for the Fram Strait on 3 January 2000. Ice concentration and thickness are obtained from the HYCOM model predictions for this day and the wave forcing comes from the WAM model. The mean ice concentration is 0.95 and the mean thickness is 2 m. The ice thicknesses have been doubled as the HYCOM predictions are known to be too low in the Fram Strait area. The initial significant wave height H_s, is shown in (a), which also shows the position of the wave mask relative to the ice edge (solid line). The mean peak period is 10.5 s, and the mean wave direction from which the waves come is 187°. Five wave directions between −9° and 221° are included with a resolution of 42.4°. The effective significant wave height, H'_s, is shown after 2.4 h (b) and 4.8 h (c). The limit of the MIZ is shown dotted in these figures. The maximum floe size after 24 h is shown in (d), and the MIZ width is approximately 24 km.

for ocean waves to do more damage to the sea ice of the polar and subpolar seas has increased (see, e.g. Prinsenberg and Peterson, 2011). And, while there is no doubt that ice-albedo feedback has been a major factor in transforming the Arctic Basin sea ice cover, it is most likely that this has been assisted by ocean waves.

Fig. 5, particularly, demonstrates considerable promise for the so-called end goal of this paper, namely to fully embed ocean wave interaction in an ice-ocean model and, prospectively, an OGCM.

ACKNOWLEDGEMENTS

The authors are grateful to the Research Council of Norway and Total E&P Norge for funding the WIFAR project, and the Universities of Otago and Adelaide for salary support. One-dimensional results are sampled from two longer manuscripts currently under review (Williams et al., 2013a,b) with additional co-authors Laurent Bertino (NERSC) and Dany Dumont (Institut des sciences de la mer de Rimouski) who are thanked for their respective contributions.

REFERENCES

Bennetts, L. G., Peter, M. A., Squire, V. A., and Meylan, M. H. (2010). "A three-dimensional model of wave attenuation in the marginal ice zone," *J Geophys Res*, Vol 115, No C12043. doi:10.1029/2009JC005982.

Bennetts, L. G., and Squire, V. A. (2009). "Wave scattering by multiple rows of circular ice floes," *J Fluid Mech*, Vol 639, pp 213–238.

Bennetts, L. G., and Squire, V. A. (2010). "Linear wave forcing of an array of axisymmetric ice floes," *IMA J Appl Math*, Vol 75, No 1, pp 108–138.

Bennetts, L. G., and Squire, V. A. (2012a). "Model sensitivity analysis of scattering-induced attenuation of ice-coupled waves," *Ocean Model*, Vol 45–46, pp 1–13.

Bennetts, L. G., and Squire, V. A. (2012b). "On the calculation of an attenuation coefficient for transects of ice-covered ocean," *Proc R Soc Lon Ser-A*, Vol 468, No 2137, pp 136–162.

Bennetts, L. G., and Williams, T. D. (2010). "Wave scattering by ice floes and polynyas of arbitrary shape," *J Fluid Mech*, Vol 662, pp 5–35.

Berry, M. V., and Klein, S. (1997). "Transparent mirrors: rays, waves and localization," *Eur J Phys*, Vol 18, No 3, pp 222–228.

Davis, N. R., and Wadhams, P. (1995). "A statistical analysis of Arctic pressure ridge morphology," *J Geophys Res*, Vol 100, No C6, pp 10915–10925.

Dumont, D., Kohout, A. L., and Bertino, L. (2011). "A wave-based model for the marginal ice zone including a floe breaking parameterization," *J Geophys Res*, Vol 116, No C04001. doi:10.1029/2010JC006682.

Gladstone, R. M., Bigg, G. R., and Nicholls, K. W. (2001). "Iceberg trajectory modeling and meltwater injection in the Southern Ocean," *J Geophys Res*, Vol 106, No C9, pp 19903–19915.

Holland, M. M., Bitz, C. M., and Tremblay, B. (2006). "Future abrupt reductions in the summer Arctic sea ice," *Geophys Res Lett*, Vol 33, No L23503. doi:10.1029/2006GL028024.

Kohout, A. L., and Meylan, M. H. (2008). "An elastic plate model for wave attenuation and ice floe breaking in the marginal ice zone," *J Geophys Res*, Vol 113, No C09016. doi:10.1029/2007JC004434.

Kwok, R., and Rothrock, D. A. (2009). "Decline in Arctic sea ice thickness from submarine and ICESat records: 1958-2008," *Geophys Res Lett*, Vol 36, No L15501. doi:10.1029/2009GL039035.

Langhorne, P. J., Squire, V. A., and Haskell, T. G. (1998). "Breakup of sea ice by ocean waves," *Ann Glaciol*, Vol 27, pp 438–442.

Langhorne, P. J., Squire, V. A., and Haskell, T. G. (2001). "Lifetime estimation for a fast ice sheet subjected to ocean swell," *Ann Glaciol*, Vol 33, pp 333–338.

Liu, A. K., and Mollo-Christensen, E. (1988). "Wave propagation in a solid ice pack," *J Phys Oceanogr*, Vol 18, No 11, pp 1702–1712.

Mahoney, A., Eicken, H., and Shapiro, L. (2007). "How fast is landfast sea ice? A study of the attachment and detachment of nearshore ice at Barrow, Alaska," *Cold Reg Sci Technol*, Vol 47, No 3, pp 233–255.

Melsom, A. (1992). "Wave-induced roll motion beneath an ice cover," *J Phys Oceanogr*, Vol 22, No 1, pp 19–28.

Perrie, W., and Hu, Y. (1996). "Air–ice–ocean momentum exchange. Part 1: Energy transfer between waves and ice floes," *J Phys Oceanogr*, Vol 26, pp 1705–1720.

Prinsenberg, S. J., and Peterson, I. K. (2011). "Observing regional-scale pack-ice decay processes with helicopter-borne sensors and moored upward-looking sonars," *Ann Glaciol*, Vol 52, No 57, pp 35–42.

Robinson, N. J., and Palmer, S. C. (1990). "A modal analysis of a rectangular plate floating on an incompressible liquid," *J Sound Vib*, Vol 142, No 3, pp 453–460.

Sakov, P., Counillon, F., Bertino, L., Lister, K. A., Oke, P. R. and Korablev, A. (2012). "TOPAZ4: an ocean-sea ice data assimilation system for the North Atlantic and Arctic," *Ocean Science*, Vol 8, pp 633–656.

Sear, C. B., and Wadhams, P. (1992). "Statistical properties of Arctic sea ice morphology derived from sidescan sonar images," *Prog Oceanogr*, Vol 29, No 2, pp 133–160.

Serreze, M. C., Holland, M. M., and Stroeve, J. (2007). "Perspectives on the Arctic's shrinking sea-ice cover," *Science*, Vol 315, No 5818, pp 1533–1536.

Shen, H. H., and Squire, V. A. (1998). "Wave damping in compact pancake ice fields due to interactions between ice cakes," In Jeffries, M., editor, *Antarctic Science Research Series*, volume 74, pages 325–341. American Geophysical Union, Washington D.C.

Squire, V. A. (2007). "Of ocean waves and sea-ice revisited," *Cold Reg Sci Technol*, Vol 49, No 2, pp 110–133.

Squire, V. A., Dugan, J. P., Wadhams, P., Rottier, P. J., and Liu, A. K. (1995). "Of ocean waves and sea ice," *Annu Rev Fluid Mech*, Vol 27, pp 115–168.

Squire, V. A., and Moore, S. C. (1980). "Direct measurement of the attenuation of ocean waves by pack ice," *Nature*, Vol 283, No 5745, pp 365–368.

Squire, V. A., Vaughan, G. L., and Bennetts, L. G. (2009). "Ocean surface wave evolvement in the Arctic Basin," *Geophys Res Lett*, Vol 36, No L22502. doi:10.1029/2009GL040676.

Strong, C. (2012). "Atmospheric influence on Arctic marginal ice zone position and width in the Atlantic sector, FebruaryApril 19792010," *Clim Dyn*, Vol 39, No 12, pp 3091–3102.

Timco, G. W., and Burden, R. P. (1997). "An analysis of the shapes of sea ice ridges," *Cold Reg Sci Technol*, Vol 25, No 1, pp 65–77.

Timco, G. W., and O'Brien, S. (1994). "Flexural strength equation for sea ice," *Cold Reg Sci Technol*, Vol 22, No 3, pp 285–298.

Timco, G. W., and Weeks, W. F. (2010). "A review of the engineering properties of sea ice," *Cold Reg Sci Technol*, Vol 60, No 2, pp 107–129.

Toyota, T., Haas, C., and Tamura, T. (2011). "Size distribution and shape properties of relatively small sea-ice floes in the Antarctic marginal ice zone in late winter," *Deep-Sea Res Pt II*, Vol 58, No 9-10, pp 1182–1193.

Toyota, T., Takatsuji, S., and Nakayama, M. (2006). "Characteristics of sea ice floe size distribution in the seasonal ice zone," *Geophys Res Lett*, Vol 33, No L02616. doi:10.1029/2005GL024556.

Vaughan, G. L., Bennetts, L. G., and Squire, V. A. (2009). "The decay of flexural-gravity waves in long sea ice transects," *Proc R Soc Lon Ser-A*, Vol 465, No 2109, pp 2785–2812.

Vaughan, G. L., and Squire, V. A. (2007). "Scattering of ice-coupled waves by a sea-ice sheet with random thickness," *Wave Random Complex*, Vol 17, No 3, pp 357–380.

Vaughan, G. L., and Squire, V. A. (2011). "Wave induced fracture probabilities for Arctic sea-ice," *Cold Reg Sci Technol*, Vol 67, No 1-2, pp 31–36.

Vaughan, G. L., Williams, T. D., and Squire, V. A. (2007). "Perfect transmission and asymptotic solutions for reflection of ice-coupled waves by inhomogeneities," *Wave Motion*, Vol 44, No 5, pp 371–384.

Vinje, T., Nordlund, N., and Kvambekk, A. (1998). "Monitoring ice thickness in Fram Strait," *J Geophys Res*, Vol 113, No C5, pp 10437–10449.

Wadhams, P., and Davis, N. R. (2000). "Further evidence of ice thinning in the Arctic Ocean," *Geophys Res Lett*, Vol 27, No 24, pp 3973–3976.

Wadhams, P., Gill, A. E., and Linden., P. (1979). "Transects by submarine of the East Greenland Polar Front," *Deep-Sea Res*, Vol 26A, pp 1311–1327.

Wadhams, P., Squire, V. A., Goodman, D. J., Cowan, A. M., and Moore, S. C. (1987). "The attenuation of ocean waves in the marginal ice zone," *J Geophys Res*, Vol 93, No C6, pp 6799–6818.

Wang, R., and Shen, H. H. (2010). "Gravity waves propagating into ice-covered ocean: a viscoelastic model," *J Geophys Res*, Vol 115, No C06024. doi:10.1029/2009JC005591.

Wang, R., and Shen, H. H. (2011). "A continuum model for the linear wave propagation in ice-covered oceans: an approximate solution," *Ocean Model*, Vol 38, No 3–4, pp 244–250.

Weber, J. E. (1987). "Wave attenuation and wave drift in the marginal ice zone," *J Phys Oceanogr*, Vol 17, No 12, pp 2351–2361.

Williams, T. D., Bennetts, L. G., and Squire, V. A. (2012). "A waves-in-ice model with a floe-breaking parameterisation," In Bingham, H. B., editor, *Proceedings 27th International Workshop on Water Waves and Floating Bodies*, page `http://www.iwwwfb.org/Workshops/27.htm`, Copenhagen, Denmark. Technical University of Denmark.

Williams, T. D., Bennetts, L. G., Squire, V. A., Dumont, D., and Bertino, L. (2013a). "Wave-ice interactions in the marginal ice zone. Part 1: theoretical foundations," *Ocean Model*, under review.

Williams, T. D., Bennetts, L. G., Squire, V. A., Dumont, D., and Bertino, L. (2013b). "Wave-ice interactions in the marginal ice zone. Part 2: Numerical implementation and sensitivity studies along 1d transects of the ocean surface," *Ocean Model*, under review.

Williams, T. D., and Porter, R. (2009). "The effect of submergence on the scattering by the interface between two semi-infinite sheets," *J. Fluids. Struct.*, Vol 25, pp 777–793.

Williams, T. D., and Squire, V. A. (2004). "Oblique scattering of plane flexural-gravity waves by heterogeneities in sea ice," *Proc R Soc Lon Ser-A*, Vol 460, No 2052, pp 3469–3497.

Williams, T. D., and Squire, V. A. (2006). "Scattering of flexural-gravity waves at the boundaries between three floating sheets with applications," *J Fluid Mech*, Vol 569, pp 113–140.

Williams, T. D., and Squire, V. A. (2007). "Wave scattering at the sea-ice/ice-shelf transition with other applications," *SIAM J Appl Math*, Vol 67, No 4, pp 938–959.

Williams, T. D., and Squire, V. A. (2010). "On the estimation of ice thickness from scattering observations," *Dynam Atmos Oceans*, Vol 49, No 2-3, pp 215–233.